

A UNIFIED BIOCHEMICAL AND CONTINUUM MECHANICAL RED BLOOD CELL MEMBRANE BILAYER – COUPLE MODEL

AMAR P. S. RANA*, SAM PAL RANA AND JAY PAL RANA

ALT.CMOS, Sunnyvale,

CA 94087 USA

email : marty@alt-cmos.com

(Received on May 14, 2004)

Abstract : We study the shapes and biochemical characteristics of human red blood cells using a unified biochemical and continuum mechanical model. In particular, we model the crenated, echinocytic shapes and show how they may shift due to changes in the pH and various amphipaths affecting the osmotic pressure by also utilizing pressure as an independent variable. In contrast to earlier works which advocate that biochemical factors may be attributable to mechanical control parameters, cytoskeletal elastic constants and effective relaxed bilayer area difference of outer plasma membrane and inner protein-based membrane skeleton, our unified model agrees well with Band 3 diffusion experimental root mean square distance data.

Key words : echinocyte

continuum mechanics

Band 3

INTRODUCTION

The normal resting shape of the human red blood cell (RBC or erythrocyte) is a flattened biconcave disc (discocyte) about 8 μm in diameter. Treatment of erythrocytes in vitro with a variety of amphipathic agents is known to transform this shape systematically and reversibly into various other shapes such as echinocytes (crenated shapes) and stomatocytes (cup-like shapes), which are further subdivided into classes labelled I, II, III (1-4). In particular, the echinocyte III is a more-or-less spherical body covered evenly with 25-50 rounded protuberances, which we shall call spicules.

The RBC membrane is composite (5, 6), the outside is the plasma membrane, a self-assembled fluid bilayer with a thickness of about 4 nm, composed of a complex mix of phospholipids, cholesterol and dissolved proteins. Lipids such as phosphatidylcholine, sphingomyelin and glycopospholipids, which are neutral at physiological pH, are common in the outer leaflet, while phosphatidylserine and phosphatidylethanolamine predominate in the inner leaflet (6, 7). Due to the negative charge of phosphatidylserine, located in the inner leaflet, there is a significant difference in charge between the two leaflets of the bilayer. Inside the plasma membrane but linked to it by protein anchors is a thin,

*Corresponding Author

two-dimensionally cross-linked protein cytoskeleton, the membrane skeleton (5, 8). The skeleton is a hexagonally linked net, each unit of which is a lamentous spectrin tetramer with an extended length of about 200 nm. The spectrin tetramer is negatively charged at physiological pH. Thermal fluctuations reduce the projected distance between the vertices of the net to about 76 nm, while the offset between the plasma membrane and the spectrin network is 30–50 nm (9, 10). Functionally, the plasma membrane serves as an osmotic barrier, passing water with relative ease but controlling, via a system of pumps and channels, the flow of ions and larger solute molecules. The membrane skeleton has the role of supporting and toughening the plasma membrane, which would otherwise disintegrate in circulatory shear flow.

Some effects are not readily explained by the purely mechanical bilayer-couple mechanism (11–15) report that RBC shape can be controlled experimentally by varying the external pH, with high pH promoting echinocyte formation and low pH, stomatocyte formation (the effect of proximity to a glass surface in promoting echinocytosis (16) is probably related to this effect). The mechanism for this effect does not seem to be well established. Some authors argue for a mechanism involving membrane proteins Band 3 has been specifically implicated (17–20). For example, it is known that high pH induces dissociation of ankyrin and Band 3, which plays a role in the linkage of the membrane skeleton to the bilayer (21). Indeed, it was shown that in vitro the membrane skeleton expands at high pH and contracts at low pH (22–23). Some amphipaths show a 100-

fold change in osmotic pressure, even when no bonds or connections between the polymer chains are altered (24). These effects can be modeled by also including pressure as an independent variable which has been ignored (25).

The present paper builds on the work of (25). We extend the Area-Difference-Elasticity (ADE) model to include the pressure term due to pH and other amphipaths affecting the osmotic pressure and also include Band 3 transient effects without advocating that somehow all biochemical effects can be solely attributed to the area difference alone.

The model

The central assumption of our work is that the red blood cell assumes a shape that minimizes its overall membrane energy subject to the appropriate constraints. We note that the ratio of the bending modulus to the shear modulus (or the stretching modulus) defines an elastic scale,

$$\Lambda_{el} = (\kappa_b/\mu)^{1/2} \quad (1)$$

Which yields $\Lambda_{el} = 0.28 \mu\text{m}$. The RBC membrane is a composite of the plasma membrane and the cytoskeletal network; correspondingly, we take the membrane energy to be a sum of two terms,

$$F = F_b + F_{el} \quad (2)$$

the bending energy,

$$F_b = \frac{1}{2} \kappa_b \int dA \mathbf{b} \cdot \mathbf{b} + C_2 - C_0 \hat{g} + \frac{\kappa \pi}{2AD^2} \int dA \mathbf{b} \cdot \mathbf{b} - \Delta A_0 \hat{g} \quad (3)$$

associated with the bilayer and an elastic energy of stretching and shear,

$$F_{el} = \frac{1}{2} K_\alpha \int \left(\frac{\Delta A}{A_0} \right)^2 \lambda_2^{-1} dA + \frac{\mu}{2} \int \left(\frac{\Delta A}{A_0} \right)^2 + \frac{\lambda_2}{\lambda_1} - 2 \int \dots \quad (4)$$

associated with the skeleton. In doing this, we treat the plasma membrane as incompressible. An estimate of its stretching modulus is K_α (bilayer) $\sim 10^{-1}$ J/m², comparable to that of a pure-phospholipid bilayer and some four orders of magnitude larger than that of the skeleton. Correspondingly, we ignore any bending rigidity associated with the isolated membrane skeleton (the dimensional estimate K_b (skeleton) $\sim K_\alpha x$ (thickness)² leaves it two orders of magnitude smaller than that of the bilayer).

Eq. 3 for the plasma membrane's contribution to the overall membrane energy is the now-standard ADE Hamiltonian (26–29). The first term was originally proposed by (30–31). C_1 and C_2 are the two local principal curvatures, C_0 is the spontaneous curvature, and the integral is over the membrane surface. The two leaflets of a closed bilayer of fixed interleaflet separation D are required by geometry to differ in area by an amount,

$$\Delta A = D \int \left(\frac{b}{2A} \right) + C_2 \int \dots \quad (5)$$

In calculations, we shall take $D \sim 3$ nm; corresponding to the distance between the neutral surfaces of the leaflets. The second term in Eq. 3 is the so-called area-difference-elasticity energy and represents the cost in stretching (or compressional) energy of the individual leaflets necessary

to force the change from the relaxed area difference ΔA_0 so as to conform to this geometric requirements. This effect occurs because a strong hydrophobic barrier prevents lipids in one leaflet from “flip-flopping” passively to the other on the time scales of mechanical shape changes. A is the area of the plasma membrane. The modulus κ' associated with the ADE term is generally of the same scale as κ_b . Note, finally, that we can substitute Eq. 5 to rewrite Eq. 3,

$$F_b = \frac{1}{2} \kappa_b \int \left(\frac{\Delta A}{A} \right)^2 + C_2 \int \dots - 2C_0 \int \left(\frac{\Delta A}{A} \right) + C_2 \int \dots \text{const} \quad (6)$$

where

$$C_0' = C_0 + \pi\alpha\Delta A_0/DA \quad (7)$$

$\alpha = \kappa'/\kappa_b$, and the constant term is shape independent. This shows that, in determining minimal shapes at given values of the control parameters, C_0 and ΔA_0 do not enter independently but only in the form of an effective spontaneous curvature C_0' or, equivalently, an effective relaxed area difference,

$$\Delta A_0' = \Delta A_0 + DAC_0'/\pi\alpha \quad (8)$$

which we shall often quote in the dimensionless, reduced form

$$\Delta a_0' = \Delta A_0'/A = \Delta a_0 + DC_0'/\pi\alpha \quad (9)$$

Note for future reference that increasing Δa_0 by 0.01 is equivalent to increasing C_0 by $6.7 \mu\text{m}^{-1}$.

Eq. 4 measures the elastic-energy cost

of the spectrin network. It depends both on the relaxed shape of the membrane skeleton and on the way it is actually distributed over the membrane surface. (The notion of a relaxed shape is, of course, somewhat nominal, since removing the skeleton from the plasma membrane (which can certainly be done (32) and would radically change its local biochemical environment, in a way which would modify its shape and elastic constants). In this redistribution, each element of the network will be stretched or compressed. The quantities λ_1 and λ_2 are the local principal extension ratios of each membrane element (33). K_α and μ are the (two-dimensional) moduli for stretch and shear, respectively and the integrals are over the undeformed shape. In writing Eq. 4, we are assuming, as appears to be typical, that the membrane skeleton does not plastically deform in the course of the experimental shape transformation being described. Note that Eq. 4 makes a particular choice of terms in the elasticity beyond those quadratic in the weak deformation parameters, $\epsilon_i = \lambda_i - 1$. For the large elastic strains which are present at narrow necks and for small spicules, these nonlinearities do play a role. As far as we are aware, RBC elasticity has not been measured well enough to produce a clear preference for a particular form of the nonlinearities. Various authors have used Eq. 4 for the elastic energy in other contexts with apparent success; however, alternative forms of the elasticity have also been proposed for dealing with problems involving large local deformations (33, 34).

In our calculations, we will identify shapes which are minima of the (free) energy defined by Eqs. 2–4 subject to

constraints of fixed membrane area A (bilayer incompressibility) and volume V (since the RBC volume is typically set by osmotic balance). Constrained minimization is achieved variationally by introducing the functional,

$$\Phi(\Sigma, P) = F + \Sigma A - PV - PAx(t); \quad (10)$$

where Σ and P are Lagrange multipliers used to enforce the surface-area and volume constraints. P is the pressure difference across the bilayer, while Σ has the dimension of a surface tension. $x(t)$ represents the root mean square distance for diffusion for Band 3. Making Φ stationary with respect to variations of membrane shape and cytoskeletal distribution leads to a set of coupled Euler-Lagrange equations. These equations can then be solved to give the shapes of mechanical equilibrium. In principle, such shapes are expected to correspond to observed equilibrium shapes at temperature $T = 0$ only; however, because the energy scale κ_b is large on the scale of $k_B T$, thermal fluctuations are generally negligible and play an important role only for “soft” modes, especially near instabilities (35). The Euler-Lagrange equations are in general nonlinear and can have multiple solutions. The lowest-energy solution for given A and V is automatically stable to small fluctuations; higher-energy solutions must be tested for stability. All local-minimum solutions are candidates for stable observable shapes, except in exceptional cases (near instability) where energy barriers become comparable to $k_B T$.

We now consider the diffusion of Band 3 and note that the pressure difference is

approximately constant until equilibrium is reached. The influx or efflux can be related to the root mean square distance dx/dt traveled due to diffusion of Band 3,

$$J = (1/\xi\delta) dx/dt = -\mathcal{J} dP/dx = -\mathcal{J} 2 \Sigma/\omega x \tag{11}$$

Where ω represents the radius for influx or efflux and ξ is the factor to convert volume removed/added with diffusion of Band 3. δ is the density of the Band 3 and \mathcal{J} is the proportionally constant. Integration of Eq. 11 gives

$$x = ((2 \mathcal{J} \delta \xi) (2\Sigma/\omega))^{1/2} t^{1/2} \tag{12}$$

The root mean square distance of diffusion due to Band 3 over time is plotted in Fig. 1 from the data from (36).

The stable shapes produced by this process depend on the control parameters: the geometrical parameters, A and V , the determinants of curvature, C_0 and ΔA_0 , which only enter in the combination Eq. 7 or, equivalently, Eqs. 8–9, the moduli, κ , κ' , K_α , and μ ; plus, finally, any parameters required to characterize the relaxed shape of the membrane skeleton. The area and volume of a typical RBC we take as (2) $A = 140 \mu\text{m}^2$ and $V = 90 \mu\text{m}^3$. The moduli are well determined by experiment. This leaves as unknown control parameters the curvature variables and the cytoskeletal parameters.

The Euler-Lagrange variational equations derived from Eq. 10 are not numerically tractable except in the case of axisymmetry, which clearly does not apply to echinocytic shapes. In this paper, we aim

to treat only fully developed echinocytic shapes (echinocyte III). For this case, individual spicules are identical and axisymmetric in shape to a good approximation and, in addition, the central body which they decorate is approximately spherical with radius R_0 . The observed distribution of spicules is rather regular, and we shall approximate the local spicule packing as a triangular array (except for special numbers of spicules, there must, of course, be some defects), which will look increasingly like an hexagonal close-packed structure, as the number of spicules, n_s , becomes large.

The base of each individual spicule, where it meets the sphere tangentially, is a circular contour L of radius r_L . If θ_L is the angle subtended by L at the center of the sphere, then

$$r_L = R_0 \sin \theta_L \tag{13}$$

Because of the close-packed structure, the circles L meet tangentially. We will describe later how to derive appropriate boundary conditions where the spicules meet the sphere. Solving the axisymmetric Euler-Lagrange equations then determines a spicule shape, including an individual spicule volume V_s and area A_s . In terms of these variables, the overall area and volume of the RBC are taken to be

$$A \approx nA_s + 0.1 \times 4\pi R_0^2 \tag{14}$$

and

$$V \approx (4\pi/3) R_0^3 + nV_s; \tag{15}$$

with the spicule number

$$n_s \approx 3.6 \times (R_0/r_L)^2 \tag{16}$$

In writing these relations, we have assumed that 10% of the spherical surface is not covered by the circular spicule bases (close packing on a flat surface would give 9.3%; curvature effects and packing defects both increase this number). The spicule volume V_s is calculated with respect to a plane through L , and Eq. 15 neglects curvature corrections. These approximations are good when the number of spicules is large, as it will turn out to be for the echinocyte shapes.

Theory

In our treatment, spicules are assumed to be axisymmetric, and individual spicules are joined to the central body along the contour L . This, our calculation involves finding a family of energy-minimizing axisymmetric spicule shapes and selecting from that family those shapes consistent with appropriate mechanical boundary conditions applied along L . The variables z and r measure distances along and perpendicular to the symmetry axis, respectively, while s measures the arclength from the pole. The function $z(r)$ determines the shape. θ is the angle between the local normal and the symmetry axis; $C_m(r)$, $C_p(r)$ are the principal curvatures,

$$C_m = d\theta/ds \text{ and } C_p = \sin\theta/r \tag{17}$$

In calculating the spicule shape, we shall assume that the relaxed cytoskeleton is locally at, a good approximation as long as the number of spicules is large, so that the spicule size is small compared to R_0 . Thus, in forming each spicule, a flat circular patch

of relaxed cytoskeleton must be elastically deformed to fit the spicule contour. We assume that this deformation is axisymmetric, so that the center of the patch remains at the apex of the spicule, and each point of the patch at relaxed radius s_0 maps to a point at arclength s and radius r on the spicule contour. The principal extension ratios can then be written,

$$\lambda_1 = r/s_0; \lambda_2 = ds/ds_0 \tag{18}$$

When these expressions for λ_1 and λ_2 are inserted into Eq. 4 we obtain an explicit form for the elastic energy in terms of the functions $s_0(s)$ and $r(s)$,

$$F_{el} = \pi K_\alpha \int_{s_0} ds_0 \left(\frac{r}{s_0} \right)^2 \left(\frac{ds}{ds_0} \right)^2 + \pi \mu \int_{s_0} ds_0 \left(\frac{r}{s_0} \right)^2 \left(\frac{ds}{ds_0} \right)^2 + \dots \tag{19}$$

Using Eqs. 2, 3, 17 and 19 we can implement the stationary condition for the free-energy functional Eq. 10 with respect to variations of membrane shape and cytoskeletal strain. This leads to a set of five coupled first-order differential equations, which are written down explicitly in the Appendix. Note that the ADE term in Eq. 3 enters only through the appearance of an effective spontaneous curvature

$$C_0^{eff} = C_0 - (\pi\alpha/DA) (\Delta A - \Delta A_0); \tag{20}$$

which must be determined self-consistently via Eq. 5.

We now turn to the boundary condition where the spicules meet the sphere. Along each element of L , the spicule membrane exerts a tension k in the plane of the

membrane and perpendicular to L, and a tension normal to the plane of the membrane. There is no tension in the third (“shear”) direction because of the membrane fluidity. In addition, the membrane skeleton exerts an independent tension which must be in-plane, since the skeleton lacks bending rigidity. In general, these tensions would be different at different points of L; however, in the axisymmetric approximation, the tensions are uniform around L and the skeletal tension is directed radially. To maintain mechanical equilibrium, these tensions must balance where the spicules meet at point A. Note that A is a point of bilateral symmetry between the two adjacent spicules, so that in-plane tensions, which act in opposite directions, always balance by symmetry. On the other hand, the normal tensions must vanish individually, since they act in the same direction. The normal tension is related to the isotropic bending moment per unit length,

$$M = \kappa_b(C_p + C_m C_0^{eff}) \tag{21}$$

Thus, an appropriate boundary condition along L is

$$d(C_p + C_m) / ds = 0 \tag{22}$$

This is the boundary condition which we shall apply in our calculations. Of course, this boundary condition is approximate, since the real spicule is only approximately axisymmetric. Indeed, with equal logic, we could argue by symmetry that normal tension should vanish at point B, where three adjacent spicules meet at a radius from the spicule axis some 15% larger than r_L .

The Euler-Lagrange equations obtained by minimizing Φ may be written down as the following set of five coupled ordinary differential equations expressing the variables s_0 , r , θ , C_m and b as functions of the arclength ‘s’:

$$2K_\alpha r ((ds/ds_0)(r/s_0) - 1) + \mu s_0 ((s_0/r) - (r/s_0) (ds_0/ds)^2 + 2r\sigma + \kappa_b r [C_p^2 - 2C_0^{eff} C_p - C_m^2] - b(s) \cos\theta + Pr^2 \sin\theta = 0; \tag{25}$$

$$dr/ds = \cos\theta \tag{26}$$

$$d\theta/ds = C_m \tag{27}$$

$$dC_m/ds = \cos\theta \sin\theta/r - C_m \cos\theta/r + Pr \cos\theta/2\kappa_b + b \sin\theta/2r\kappa_b \tag{28}$$

$$db/ds = 2K_\alpha ((ds/ds_0)(r/s_0) - 1) + \mu s_0 (ds_0/ds)((1/s_0)(ds_0/ds) - (s/r^2)(ds/ds_0)) + 2\sigma + \kappa_b [c_m^2 - 2C_0^{eff} C_m - C_p^2] + 2pr \sin\theta \tag{29}$$

Here $b(s)$ is a local variable introduced to impose the constraint, $dr/ds = \cos\theta$, as first suggested by (38). The variables s , s_0 , r , θ and b vanish at the North pole. Note also that the surface tension σ used in these equations is, in general, shifted from the parameter Σ appearing in Eq. 10.

Substituting Eq. 17 and 27 into 22, differentiating $b(s)$ with respect to ‘s’, and equating (after removing small terms with $\kappa_b = 2.0 \times 10^{-19} J$ (38–39) from Eq. 29 and rearranging, we get the spicule radius r_L dependent on pressure p as,

$$r_L = (2p \sin^3\theta \pm (4p^2 \sin^6\theta - 8\sigma p \sin^2\theta (C_m - \cos^2\theta \sin\theta))^{1/2}) / 2p (C_m - \cos^2\theta \sin\theta) \tag{30}$$

We combine the r_L due to the area difference Δa_0 Eq. 16 as well as pressure Eq. 30 and plot it in Fig. 2 which shows n_s ,

spicule number as a function of $\Delta a_0'$ for area difference effects and added pressure term for biochemical effects. We assume a value of $C_m = 1/0.28 (\mu\text{m})^{-1}$ for spicules from Eq. 1.

RESULTS

Figure 1 shows the parabolic dependence of the root mean square distance of diffusion due to Band 3 over time with the data taken from (36).

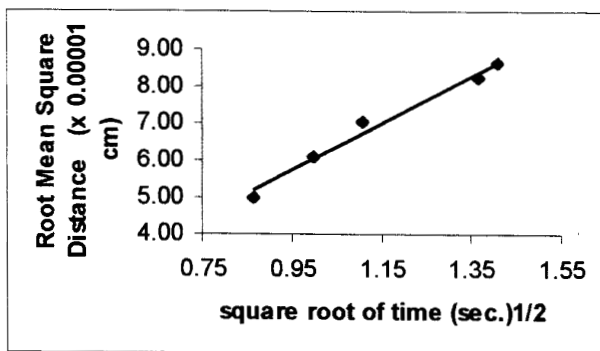


Fig. 1: Parabolic dependence of the root mean square distance of diffusion due to Band 3 over time with data taken from (35).

Figure 2 shows that biochemical effects as interpreted via the pressure term show an increase in spicule number with pressure in agreement with the experimental observation of some amphipaths favoring the echinocyte shape.

The continuum model (25) by itself utilizes the experimentally unproven bilayer area difference as the sole parameter of echinocyte spicules formation. We show that when pressure is also included as an independent variable, the

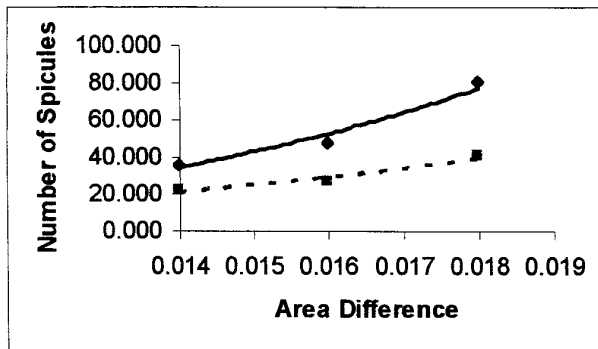


Fig. 2: Calculated equilibrium number of spicules n_s plotted as a function of the reduced effective relaxed area difference $\Delta a_0'$ and the shift in n_s due to increase in pressure (solid line) due to changes in pH or amphipaths which affect osmotic pressure.

echinocyte spicules are preferred, which also has been observed experimentally (22-24).

DISCUSSION

The fully developed echinocyte III at equilibrium spicule number as calculated according to the program outlined additionally utilizes pressure as an independent variable. The internal dynamics may also play a significant role in influencing the RBC shapes without appreciable effect on the pressure. In such cases, additional parameters need to be incorporated into the model.

The success of this unified approach strengthens the hypothesis that RBC shapes can be understood on the basis of continuum mechanics and biochemical content. The crenated, echinocytic shapes shift due to changes in the pH and various amphipaths affecting the osmotic pressure have been shown by calculating the spicule numbers

from the Euler-Lagrange equations by additionally including pressure as an independent variable rather than simply claiming it be attributed to the effective relaxed bilayer area difference of outer plasma membrane and inner protein-based membrane skeleton. Our unified model agrees well with Band 3 diffusion experimental root mean square distance

data. We hope that the research for new medications may also take into account the effect of RBC shapes.

ACKNOWLEDGEMENTS

We greatly appreciate the assistance of Mr. John P. Sheehy in editing the manuscript.

REFERENCES

- Brecher G, Bessis M. Present status of spiculated red cells and their relationship to the discocyte-echinocyte transformation: A critical review. *Blood* 1972; 40: 333-344.
- Bessis M. Living Blood Cells and their Ultrastructure, tr. RI Weed. Springer-Verlag, New York, 1973.
- Chailley B, Weed RI, Leblond PF, Maigne J. Formes échinocytaires et stomatocytaires du globule rouge. *Nouv Rev fr Hemat* 1973; 13: 71-87.
- Mohandas N, Feo C. A quantitative study of the red cell shape changes produced by anionic and cationic derivatives of phenothiazines. *Blood Cells* 1975; 1: 375-384.
- Steck TL. In Cell Shape: Determinants, Regulation, and Regulatory Role. W.D. Stein and F. Bronner, editors. *Academic Press, San Diego* 1989; 205-246.
- Alberts B, Bray D, Lewis J, Ra M, Roberts K, Watson JD. Molecular Biology of the Cell, 3rd ed., Chs. 10 and 16. Garland Publishing, New York, 1994.
- Gennis RB. Biomembranes: Molecular Structure and Function. Chapter 4. Springer-Verlag, New York, 1989.
- Bennett V. Spectrin-based membrane skeleton: A multipotential adaptor between plasma membrane and cytoplasm. *Physiol Rev* 1990; 70: 1029-1065.
- Byers TJ, Branton D. Visualization of the protein associations in the erythrocyte membrane skeleton. *Proc Natl Acad Sci (USA)* 1985; 82: 6153-6157.
- Liu SC, Derick LH, Palek J. Visualization of the hexagonal lattice in the erythrocyte membrane skeleton. *J Cell Biol* 1987; 104: 527-536.
- Weed RI, Chailley B. Calcium-pH interactions in the production of shape change in erythrocytes. *Nouv Rev fr Hemat* 1972; 12: 775-788.
- Gedde MM, Yang E, Huestis WH. Shape response of human erythrocytes to altered cell pH. *Blood* 1995; 4: 1595-1599.
- Gedde MM, Huestis WH. Membrane potential and human erythrocyte shape. *Biophys J* 1997a; 72: 1220-1233.
- Gedde MM, Davis DK, Huestis WH. Cytoplasmic pH and human erythrocyte shape. *Biophys J* 1997b; 72: 1234-1246.
- Gedde MM, Yang E, Huestis WH. Resolution of the paradox of red cell shape changes in low and high pH. *Biochim Biophys Acta* 1999; 1417: 246-253.
- Furchgott RF, Ponder E. Disk-sphere transformation in mammalian red cells II. The nature of the anti-sphering factor. *J Exp Biol* 1940; 17: 117-127.
- Gimsa J, Ried C. Do band 3 protein conformational changes mediate shape changes of human erythrocytes? *Mol Membr Biol* 1995; 12: 247-254.
- Jay DG. Role of band 3 in homeostasis and cell shape. *Cell* 86: 853-854. Landman KA. A continuum model for a red blood cell transformation: Sphere to crenated sphere. *J Theor Biol* 1996; 106: 329-351.
- Gimsa J. A possible molecular mechanism governing human erythrocyte shape. *Biophys J* 1998; 75: 568-569.
- Hägerstrand H, Danieluk M, Bobrowska-Hägerstrand M, Iglıc A, Wróbel A, Isomaa B,

- Nikinmaa M. Influence of band 3 protein absence and skeletal structures on amphiphile- and Ca^{2+} -induced shape alterations in erythrocytes: a study with lamprey (*Lampetra uviatilis*), trout (*Onchorhynchus mykiss*), and human erythrocytes. *Biochim Biophys Acta* 2000; 1466: 125–138.
21. Low PS, Willardson BM, Mohandas N, Rossi M, Shohet S. Contribution of the band 3-ankyrin interaction to erythrocyte membrane mechanical stability. *Blood* 1991; 77: 1581–1586.
 22. Elgsaeter A, Stokke BT, Mikkelsen A, Branton D. The Molecular Basis of Erythrocyte Shape. *Science* 1986; 234: 1217–1223.
 23. Stokke BT, Mikkelsen A, Elgsaeter A. Spectrin, human erythrocyte shapes, and mechanochemical properties. *Biophys J* 1986; 49: 319–327.
 24. Tanaka T, Fillmore D, Sun ST, Nishio I, Swislow G, Shah A. Phase Transitions in Ionic Gels. *Phys Rev Lett* 1980; 45, 20: 1636–1639.
 25. Lim GHW, Wortis M, Mukhopadhyay R. Stomatocyte-discocyte-echinocyte sequence of the human red blood cell: Evidence for the bilayer-couple hypothesis from membrane mechanics. *Proc Natl Acad Sci* 2002; 99: 26: 16766–16769.
 26. Svetina S, Brumen M, Žekš B. Lipid bilayer elasticity and the bilayer couple interpretation of red cell shape transformations and lysis. *Stud Biophys* 1985; 110: 177–187.
 27. Bòžić B, Svetina S, Žekš B, Waugh RE. Role of lamellar membrane structure in tether formation from bilayer vesicles. *Biophys J* 1992; 61: 963–973.
 28. Wiese W, Harbich W, Helfrich W. Budding of lipid bilayer vesicles and at membranes. *J Phys Condens Matter* 1992; 4: 1647–1657.
 29. Miao L, Seifert U, Wortis M, Döbereiner HG. Budding transitions of fluid-bilayer vesicles: the effect of area-difference elasticity. *Phys Rev E* 1994; 49: 5389–5407.
 30. Helfrich W. Elastic properties of lipid bilayers: theory and possible experiments. *Z Naturforsch* 1973; C28: 693–703.
 31. Deuling HJ, Helfrich W. The curvature elasticity of fluid membranes: A catalogue of vesicle shapes. *J Phys (Paris)* 1976; 37: 1335–1345.
 32. Sheetz MP. DNase-I-dependent dissociation of erythrocyte cytoskeletons. *J Cell Biol* 1979; 81: 266–270.
 33. Evans EA, Skalak R. *Mechanics and Thermodynamics of Biomembranes*. CRC Press, Boca Raton, 1980.
 34. Discher DE, Mohandas N, Evans EA. Molecular maps of red cell deformation: hidden elasticity and in situ connectivity. *Science* 1994; 266: 1032–1035.
 35. Wortis M, Jarić M, Seifert U. Thermal shape fluctuations of fluid-phase phospholipid-bilayer membranes and vesicles. *J Mol Liq* 1997; 71: 195–207.
 36. Tomishige M, Sako Y, Kusumi A. Regulation mechanism of the lateral diffusion of Band 3 in erythrocyte membranes. *J Cell Biology* 1998; 142: 4: 989–1000.
 37. Peterson MA. An instability of the red blood cell shape. *J Appl Phys* 1985; 57: 1739–1742.
 38. Waugh RE, Bauserman RG. Physical measurements of bilayer-skeletal separation forces. *Ann Biomed Eng* 1995; 23: 308–321.
 39. Strey H, Peterson M, Sackmann E. Measurement of erythrocyte membrane elasticity by flicker eigen-mode decomposition. *Biophys J* 1995; 69: 478–488.